



## Cracked components under anti-plane loading: recent outcomes and future developments

F. Berto

*Norwegian University of Science and Technology - NTNU, Department of Engineering Design and Materials, Trondheim, 7491, Norway*

**ABSTRACT.** The existence of three-dimensional effects at cracks has been known for many years, but understanding has been limited, and for some situations still is. Understanding improved when the existence of corner point singularities and their implications became known. Increasingly powerful computers made it possible to investigate three-dimensional effects numerically in detail. Despite increased understanding, three-dimensional effects are sometimes ignored in situations where they may be important. The purpose of the present investigation is to study by means of accurate 3D finite element (FE) models a coupled fracture mode generated by anti-plane loading of a straight through-the-thickness crack in linear elastic plates. An extended version of the present work has recently been published in the literature.

The results obtained from the highly accurate finite element analyses have improved understanding of the behaviour of through cracked components under anti-plane loading. The influence of plate bending is increasingly important as the thickness decreases. It appears that a new field parameter, probably a singularity, is needed to describe the stresses at the free surfaces. Discussion on whether  $K_{III}$  tends to zero or infinity as a corner point is approached is futile because  $K_{III}$  is meaningless at a corner point.

The intensity of the local stress and strain state through the thickness of the cracked components has been evaluated by using the strain energy density (SED) averaged over a control volume embracing the crack tip. The SED has been considered as a parameter able to control fracture in some previous contributions and can easily take into account also coupled three-dimensional effects. Calculation of the SED shows that the position of the maximum SED is independent of plate thickness. Both for thin plates and for thick ones the maximum SED is close to the lateral surface, where the maximum intensity of the coupled mode II takes place.

**KEYWORDS.** Fracture mechanics; Finite element analysis; Anti-plane loading; Stress intensity factor; Corner point effects.



**Citation:** Berto, F., Cracked components under anti-plane loading: recent outcomes and future developments, *Frattura ed Integrità Strutturale*, 41 (2017) 475-483.

**Received:** 15.05.2017

**Accepted:** 26.07.2017

**Published:** 01.07.2017

**Copyright:** © 2017 This is an open access article under the terms of the CC-BY 4.0, which permits unrestricted use, distribution, and reproduction in any medium, provided the original author and source are credited.



## INTRODUCTION

Crack tip surface displacements in the vicinity of a corner point in which a crack front intersects a surface are often of practical interest. Assuming that Poisson's ratio,  $\nu > 0$ , then kinematics considerations for an antisymmetric loading [1-2] show that modes II and III crack tip surface displacements cannot exist in isolation. Mode II induces mode III<sup>c</sup> and mode III induces mode II<sup>c</sup>. These induced modes are sometimes called coupled modes, indicated by the superscript c.

The existence of three-dimensional effects at cracks has been known for many years [3,4], but understanding has been limited, and for some situations still is. Understanding improved when the existence of corner point singularities [5] and their implications became known [6]. Despite increased understanding, three-dimensional effects are sometimes ignored in situations where they may be important.

Within the framework of linear elastic fracture mechanics [7] the stress field in the vicinity of a crack tip is dominated by the leading term of a series expansion of the stress field [8]. This leading term is the stress intensity factor,  $K$ . In three dimensional geometries, the derivation of stress intensity factors makes the implicit assumption that a crack front is continuous. This is not the case in the vicinity of a corner point, and the nature of the crack tip singularity changes. The resulting corner point singularities were described in detail in 1979 by Bažant and Estenssoro [5]. Some additional results were given by Benthem in 1980 [9]. For corner point singularities, the polar coordinates in Fig. 1 are replaced by spherical coordinates  $(r, \theta, \phi)$  with origin at the corner point. The angle  $\phi$  is measured from the crack front.

There do not appear to be any exact analytic solutions for corner point singularities. In their analysis Bažant and Estenssoro [5] assumed that all three modes of crack tip surface displacement are of the form  $r^\lambda \rho^p F(\theta, \phi)$ , where  $\rho$  is distance from the crack tip, and  $p$  is a given constant. They then calculated  $\lambda$  numerically for a range of situations:  $\lambda$  is a function of Poisson's ratio,  $\nu$ . For the antisymmetric mode,  $\lambda = 0.598$  for  $\nu = 0.3$ . Benthem [9] made an equivalent assumption but used a different numerical method to calculate  $\lambda$ . The stress intensity measure,  $K_\lambda$ , may be used to characterise corner point singularities, where  $\lambda$  can be regarded as a parameter defining the corner point singularity. However, expressions for numerical values of  $K_\lambda$ , and associated stress and displacement fields, do not appear to be available. At the present state of the art the extent of a corner point singularity dominated region has to be determined numerically.

At a corner point stresses are a singularity. They must be either infinite or zero,  $\lambda$  is indeterminate, and it is reasonable to speak of stress intensity factors in an asymptotic sense [3]. In the limit, as a crack front is approached, displacement fields must be those of a stress intensity factor [9]. Hence, there is an infinitesimal  $K$ -dominated region within the core region of a corner point singularity. The stress intensity factors are proportional to  $s^{0.5 - \lambda}$  where  $s$  is the distance from the surface along the  $z$  axis [9]. Hence, for the antisymmetric mode  $K_{II}$  and  $K_{III}$  both tend to infinity as a corner point is approached. Further, as a corner point the ratio  $K_{III}/K_{II}$  tends to a limiting value which is a function of  $\nu$ . For  $\nu = 0.3$  the limiting ratio is 0.5 [9]. Benthem points out that  $K_{II}$  and  $K_{III}$  lose their meaning at a corner point [9]. Dhondt suggests that modes II<sup>c</sup> and III<sup>c</sup> might not be singular [10]. The predicted tendency to infinity is reasonable for  $K_{II}$  since relevant stresses are in plane and disclinations are zero [3]. From a linear elastic viewpoint the predicted tendency of  $K_{III}$  to infinity cannot be correct [4]. At a surface shear stresses perpendicular to the surface are zero, which implies that  $K_{III}$  tends to zero as the surface is approached. Mode III is a torsion problem [11]. Under mode III (anti-plane) loading initially plane cross sections, including the surface at a corner point, do not remain plane under load [4] and disclinations appear. It is well known that serious error can arise if warping of non-circular cross sections under torsion is not taken into account in stress analyses [12]. Warping of the surface under mode III means that  $\tau_{yz}$  at the surface does not have to be zero, and finite values of  $K_{III}$  are possible. The implication is that the non linearities cannot be regarded as being in a core region within a corner point singularity dominated region and that Bažant and Estenssoro's prediction that  $K_{III}$  tends to infinity as a corner point is correct. The alternative view, which is supported by a large body of evidence [4], is that apparent values of  $K_{III}$  decrease towards the surface in the  $z$  direction. This implies that  $K_{III}$  tends to zero as a corner point is approached, which is intuitively correct. It also implies that non linearities can be regarded as being within a core region, but does not explain why Bažant and Estenssoro's analysis does not give the correct limit. Nevertheless, this alternative view may well be adequate when considering practical implications. This paradox needs to be resolved so that the results of finite element analysis can be interpreted correctly.

There does not appear to have been a systematic investigation of the extent to which Bažant and Estenssoro's initial assumption is justified. Their assumption does appear to be satisfactory for the symmetric mode (mode I) in that their analysis leads to useful results [4]. The purpose of the present investigation is to study a coupled fracture mode generated

by anti-plane loading of a straight through-the-thickness crack in linear elastic plates by means of accurate three-dimensional finite element (FE) models. An extended version of the present work has recently been published in the literature [3]. The material is assumed to be a homogeneous isotropic continuum, and its behaviour is assumed to be linearly elastic.

Due to the uncertainties in the definition of the stress intensity factors on the free surfaces, as stated above, the strain energy averaged in a control volume (SED) has been employed in the present contribution to quantify the stress intensity through the thickness of the plate. For a review of the SED the reader can refer to [13]. This parameter has been successfully used by Lazzarin and co-authors to assess the fracture strength of a large bulk of materials, characterized by different control volumes, subjected to wide combinations of static loading [14 - 16] and the fatigue strength of notched components [17, 18]. As described in [13, 19] an intrinsic advantage of the SED approach is that it permits automatically to take into account higher order terms and three-dimensional effects. The parameter is easy to calculate in comparison with other well-defined and suitable 3D parameters [20, 21] and can be directly obtained by using coarse meshes [13, 19]. Another advantage of the SED is that it is possible to easily understand whether the through-the-thickness effects are important or not in the fracture assessment for a specific material characterized by a control volume depending on the material properties. Some brittle materials are characterized by very small values of the control radius and are very sensitive to stress gradients also in a small volume of material [13]. On the other hand more ductile materials have the capability of stress averaging in a larger volume and for this reason are less sensitive to the variations of the stress field through the thickness of the plate. The SED, once the control volume is properly modeled through the thickness of the plate, is able to quantify the 3D effects in comparison with the sensitivity of the specific material so providing precious information for the fracture assessment.

## FINITE ELEMENT MODELLING

In the present calculations, stresses, stress intensity factors and displacements are examined in detail for 100 mm square plates of various thicknesses under anti-plane (nominal mode III) loading. One half of the plate geometry used is shown in Fig. 2. The thickness is  $t$ . A through thickness crack has its tip at the centre of the plate, so its length,  $a$ , is 50 mm. Calculations are carried out using ANSYS 11 for  $t/a = 0.25, 0.5, 0.75, 1, 1.25, 1.5, 1.75, 2, 2.25, 2.5, 2.75$  and 3. Poisson's ratio is taken as 0.3 and Young's modulus as 200 GPa. A displacement of  $10^{-3}$  mm is applied to the edge of the plate. Stress intensity factors are calculated from stresses on the crack surface near the crack tip using standard equations [7,11]. The strain energy density is calculated from a control volume at the crack tip. One quarter of the plate is modelled. An overall view of the finite element mesh is shown in Fig. 3. Details of the mesh at the outer surface and crack tip are shown in the figure.

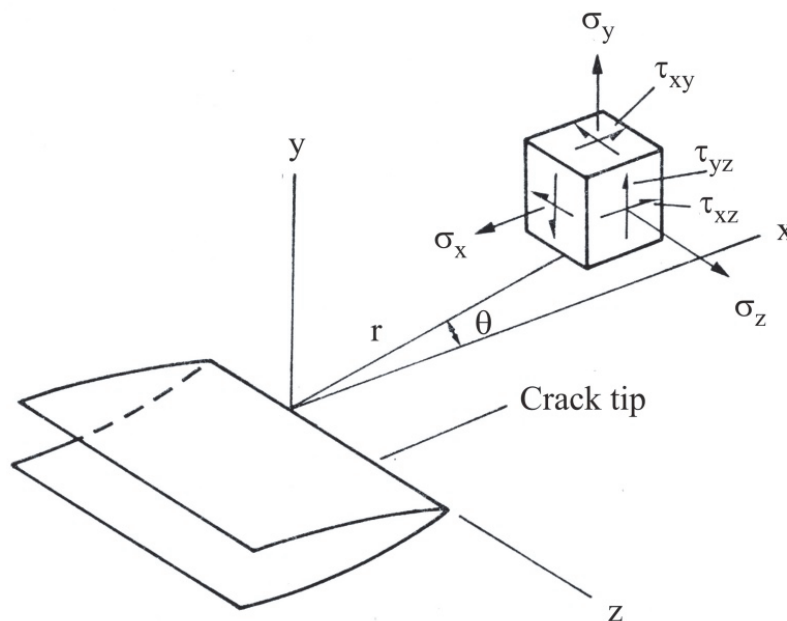


Figure 1: Notation for crack tip stress field.

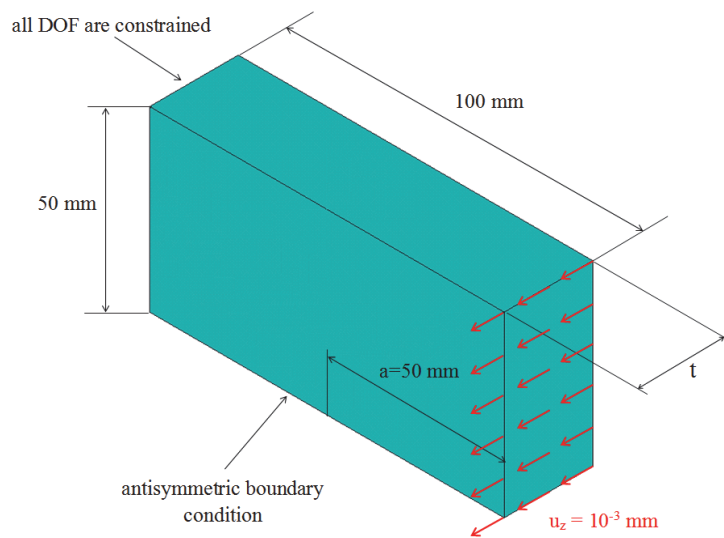


Figure 2: Plate geometry.

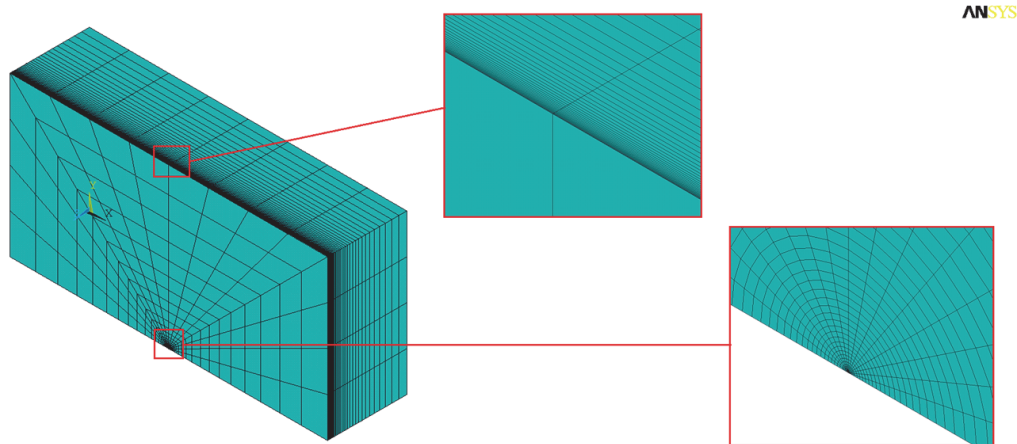


Figure 3: Overall view of finite element mesh. Detail of finite element mesh at outer surface and at crack tip.

## RESULTS

Crack surface stresses,  $\tau_{yz}$  and  $\tau_{xy}$  (Fig. 1) were extracted from the finite element results at distances,  $s$ , from the plate surfaces of 0 mm, 0.25 mm, 1 mm and 2 mm. Results for  $t/a = 1$ , plotted on logarithmic scales, are shown in Figs. 4-6. Results for other values of  $t/a$  are generally similar, but with some differences in detail. When the plot is a straight line its slope is  $-\lambda$ . Values of  $\lambda$  taken from straight line plots are shown in Tabs. 1 and 2. Where no value is shown the plot could not be regarded as a straight line.

For  $s = 0.25$  mm, 1 mm and 2 mm  $\lambda$  calculated from  $\tau_{xy}$  is close to the theoretical value of 0.5 for a stress intensity factor singularity (Tab. 1). Hence, realistic values of  $K_{II}$  can be calculated. For  $s = 0$  mm the value of  $\lambda$  has a maximum for  $t/a = 0.25$ , and decreases as  $t/a$  increases. The values of  $\lambda$  are all significantly less than the theoretical value of 0.598 for a corner point singularity. Realistic values of  $K_{II}$  can probably be calculated for  $t/a > 2$ .

Realistic values of  $K_{III}$  can be calculated from  $\tau_{yz}$  for  $s = 1$  mm and 2 mm. The results for  $s = 0$  mm (Fig. 4) show that  $\tau_{yz}$  is slightly lower than  $\tau_{xy}$  for small  $x$ , and decreases as  $x$  increases. Realistic values of  $K_{III}$  cannot be calculated. The presence of finite values of  $\tau_{yz}$ , linked to finite values of  $K_{III}$ , appears because of the appearance of mode I disclinations, which are rotations about the  $y$  axis. Differentiating the expression for the displacement  $U_z$  gives the amount of this rotation which increases towards the crack tip, with a concomitant increase in  $\tau_{yz}$  at a surface. This accounts qualitatively for the observed distributions of  $\tau_{yz}$  at a surface.



| $t/a$ | $s = 0$ mm | $s = 0.25$ mm | $s = 1$ mm | $s = 2$ mm |
|-------|------------|---------------|------------|------------|
| 0.25  | 0.538      | 0.498         | 0.497      | 0.497      |
| 0.5   | 0.527      | 0.498         | 0.497      | 0.497      |
| 0.75  | 0.523      | 0.498         | 0.497      | 0.497      |
| 1     | 0.520      | 0.498         | 0.497      | 0.497      |
| 1.25  | 0.517      | 0.498         | 0.497      | 0.497      |
| 1.5   | 0.515      | 0.498         | 0.497      | 0.497      |
| 1.75  | 0.513      | 0.498         | 0.497      | 0.497      |
| 2.    | 0.512      | 0.498         | 0.497      | 0.497      |
| 2.25  | 0.510      | 0.498         | 0.497      | 0.497      |
| 2.5   | 0.510      | 0.498         | 0.497      | 0.497      |
| 2.75  | 0.509      | 0.498         | 0.497      | 0.497      |
| 3     | 0.508      | 0.498         | 0.497      | 0.497      |

Table 1: Values of  $\lambda$  for  $\tau_{xy}$ ,  $s$  is the distance from surface in the  $z$  direction.

| $t/a$ | $s = 0$ mm | $s = 0.25$ mm | $s = 1$ mm | $s = 2$ mm |
|-------|------------|---------------|------------|------------|
| 0.25  | -          | -             | 0.507      | 0.504      |
| 0.5   | -          | -             | 0.506      | 0.503      |
| 0.75  | -          | -             | 0.506      | 0.502      |
| 1     | -          | -             | 0.506      | 0.502      |
| 1.25  | -          | -             | 0.506      | 0.502      |
| 1.5   | -          | -             | 0.506      | 0.502      |
| 1.75  | -          | -             | 0.506      | 0.502      |
| 2     | -          | -             | 0.506      | 0.502      |
| 2.25  | -          | -             | 0.506      | 0.502      |
| 2.5   | -          | -             | 0.505      | 0.502      |
| 2.75  | -          | -             | 0.506      | 0.502      |
| 3     | -          | -             | 0.506      | 0.502      |

Table 2: Values of  $\lambda$  for  $\tau_{yz}$ ,  $s$  is the distance from surface in the  $z$  direction.

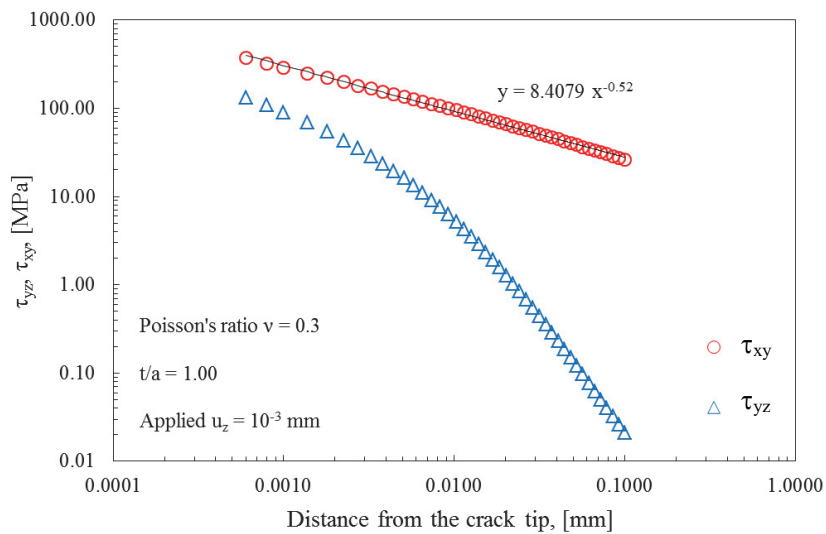


Figure 4: Stresses  $\tau_{yz}$  and  $\tau_{xy}$  on crack surface at  $s = 0$  mm from plate surface,  $t/a = 1$ .

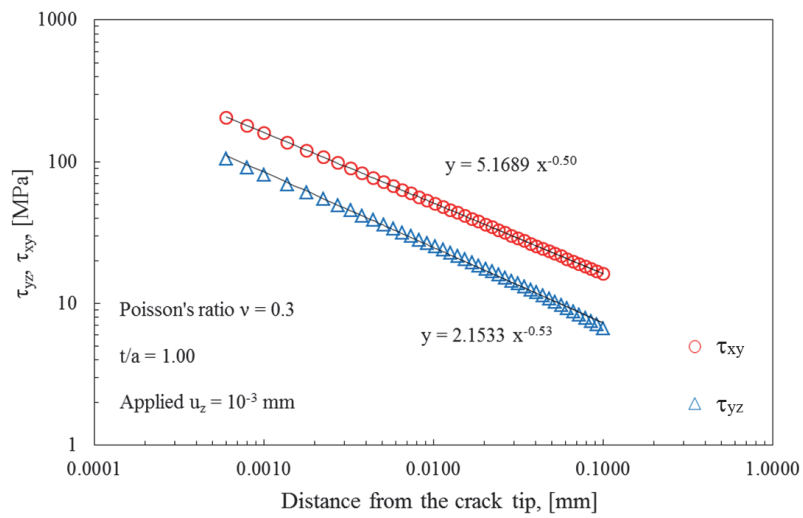


Figure 5: Stresses  $\tau_{yz}$  and  $\tau_{xy}$  on crack surface at  $s = 0.25$  mm from plate surface,  $t/a = 1$ .

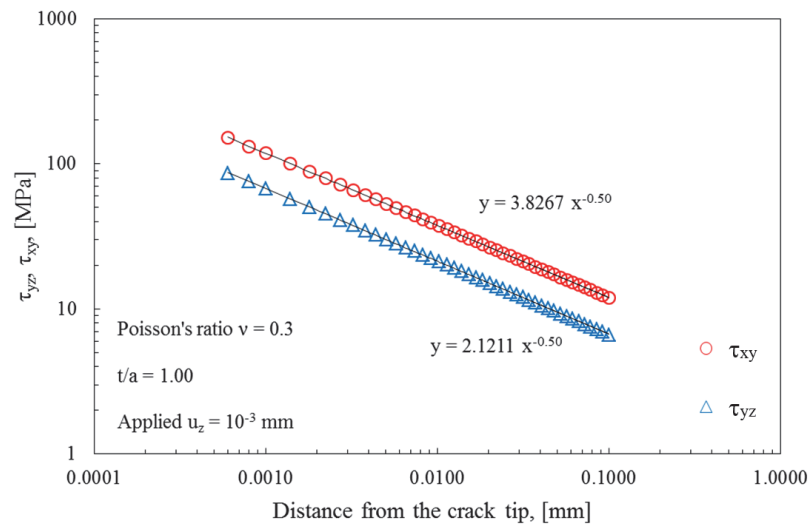


Figure 6: Stresses  $\tau_{yz}$  and  $\tau_{xy}$  on crack surface at  $s = 2$  mm from plate surface,  $t/a = 1$ .

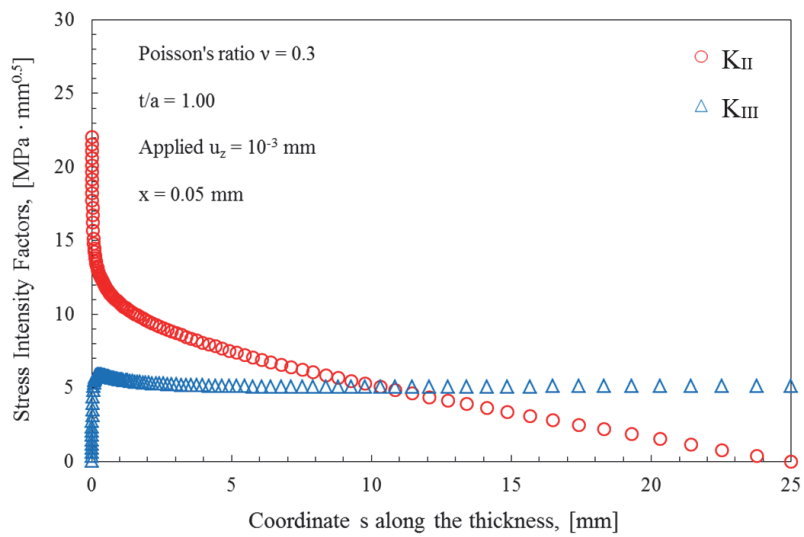


Figure 7: Through thickness distribution of  $K_{II}$  and  $K_{III}$  for:  $t/a = 1$ ,  $x = 0.05$  mm.



Through-the-thickness distributions of  $K_{II}$  and  $K_{III}$  for  $t/a = 1$  is shown in Fig. 7. From Tabs. 1 and 2 the values of  $K_{II}$  are not realistic for  $s < 0.25$  mm and the values of  $K_{III}$  are not realistic for  $s < 1$  mm.

The distribution of  $K_{III}$  presents a maximum at the centre line, but  $K_{III}$  then remains nearly constant for about half the distance to the plate surface. The influence of plate bending means that maxima steadily decrease as  $t/a$  decreases. As a surface is approached  $K_{III}$  first decreases slightly then increases to a maximum at about 0.15 mm from the surface. There is then an abrupt drop which is within the region where realistic values of  $K_{III}$  cannot be calculated.

Plate bending theory [2] suggests that  $K_{II}$  should be zero on the centre line, with a linear increase towards a surface.  $K_{II}$  does indeed increase linearly for much of the thickness with a greater increase as the surface is approached. This is within the region where realistic values of  $K_{II}$  cannot be calculated. The extent of the linear portion, in terms of plate thickness, decreases as  $t/a$  increases but is still present when  $t/a = 3$ . Maximum values of  $K_{II}$  are at the surface. This is within the region where calculated  $K_{II}$  values are not realistic so caution is needed in the interpretation of results.

## DISCUSSION

There has been a lot of discussion on whether  $K_{III}$  tends to zero or infinity as a corner point is approached [3]. When apparent  $K_{III}$  values are calculated from stresses at a constant distance from the crack tip then  $K_{III}$  appears to tend to zero as the model surface is approached (Fig. 7), in accordance with the linear elastic prediction. However, apparent values of  $K_{III}$  at the surface, linked to finite values of  $\tau_{yz}$  (Fig. 4), increase strongly as the distance from the crack tip at which they are calculated decreases. These results can be interpreted as indicating that  $K_{III}$  tends to infinity at a corner point in accordance with Bažant and Estenssoro's prediction. The results in Fig. 7 also show that  $K_{II}$  does appear to tend to infinity as the surface is approached, in accordance with Bažant and Estenssoro's prediction. The discussion is futile because, as pointed out by Benthem [9],  $K_{III}$  is meaningless at a corner point and there is no paradox. For  $s \geq 0.2$  mm  $\lambda$  calculated from  $\tau_{xy}$  is close to the theoretical value of 0.5 for a stress intensity factor singularity so  $K_{II}$  provides a reasonable description of the crack tip stress field. Similarly,  $K_{III}$  provides a reasonable description of the crack tip stress field for  $s \geq 1$  mm. At the surface values of  $\lambda$  obtained from  $\tau_{xy}$  are always less than the theoretical value for a corner point singularity, and decrease with increasing plate thickness. The distribution of  $\tau_{yz}$  at the surface (Fig. 4) cannot be accounted for on the basis of Bažant and Estenssoro's analysis. There is clear evidence of a boundary layer effect whose extent is independent of plate thickness. The only available characteristic dimension controlling the boundary layer thickness is the crack length,  $a$ .

## STRAIN ENERGY DENSITY THROUGH THE PLATE THICKNESS

The intensity of the local stress and strain state through the plate thickness can be easily evaluated by using the strain energy density (SED) averaged over a control volume embracing the crack tip (see Ref. [13] for a review of the SED approach). The main advantage with respect to the local stress-based parameters is that it does not need very refined meshes in the close neighbourhood of the stress singularity [19]. Furthermore the SED has been considered as a parameter able to control fracture and fatigue in some previous contributions [14-16, 34-35] and can easily take into account also coupled three-dimensional effects [4,22].

With the aim to provide some numerical assessment of the contribution of the three-dimensional effects, specifically the coupled fracture mode,  $K_{II}$ , the local energy density through the plate thickness is evaluated and discussed in this section.

Fig. 8 shows the local SED variation across the plate averaged over a cylindrical volume having radius  $R_0$  and height  $h$ , with  $h$  about equal to  $R_0$ . In Refs [13, 14-16, 17-18]  $R_0$  was thought of as a material property which varies under static and fatigue loading but here, for the sake of simplicity,  $R_0$  and  $h$  are simply set equal to 1.0 mm, only to quantify the three-dimensional effects through the disc thickness.

The influence of the applied mode III loading combined with the induced singular mode II loading is shown in Fig. 8. It is evident that the position of the maximum SED is the same in all cases. It is close to the lateral surface, where the maximum intensity of the coupled mode II takes place, both for thin plates,  $t/a=0.5$  and 1.0, and for thick ones,  $t/a=2$  and 3. In fact, as can be seen from Fig. 7, the maximum contribution of the coupled mode II, at the lateral surface, is significantly higher (about 4 times) compared to the maximum contribution of the applied mode III, at the mid plane.

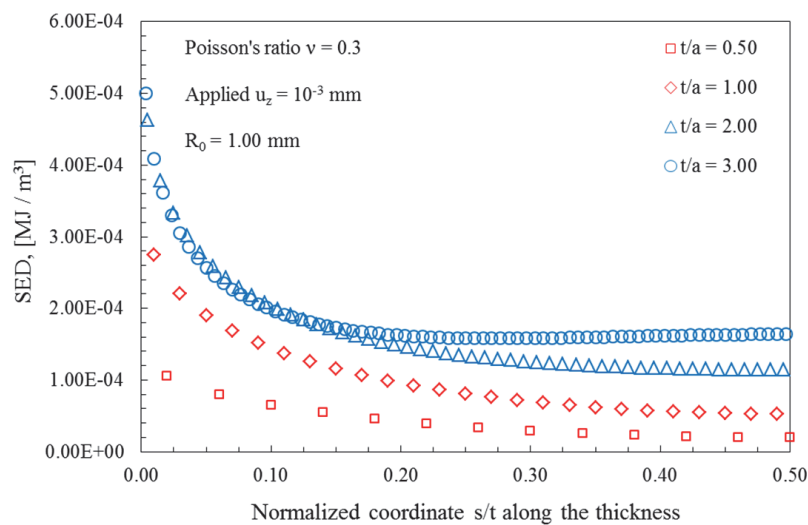


Figure 8: Through the thickness *SED* distribution for  $t/a = 0.50, 1, 2, 3$ . Control radius  $R_0 = 1.00$  mm.

## CONCLUSIONS

- (1) The results obtained from the highly accurate finite element analyses have improved understanding of the behaviour of through cracked plates under anti-plane loading. In particular, it is confirmed that mode III does induce coupled mode II<sup>c</sup>.
- (2) The influence of plate bending is increasingly important as plate thickness decreases. The anti-plane loading used is a nominal mode III loading. For thin plate it is a mixed modes III and II loading, in which mode III induces mode II<sup>c</sup> and vice versa. At the present state of the art it is not possible to separate the coupled modes from the applied modes.
- (3) Bažant and Estenssoro's analysis works well for the symmetric mode (mode I), but it is incomplete for the asymmetric mode (a combination of modes II and III).
- (4) Discussion on whether  $K_{III}$  tends to zero or infinity as a corner point is approached is futile because, as pointed out by Benthem,  $K_{III}$  is meaningless at a corner point.
- (5) The present results do not confirm the existence of a corner point singularity dominated region within a  $K$ -dominated region. It appears that a new field parameter, probably a singularity, is needed to describe the stresses at the plate surfaces.
- (6) Calculation of the strain energy density (SED) in a control volume at the crack tip shows that the position of the maximum SED is independent of plate thickness. Both for thin plates and for thick ones the maximum SED is close to the lateral surface, where the maximum intensity of the coupled mode II takes place.
- (7) Under the anti-plane loading used theoretical understanding of the stress field in the vicinity of a corner point is still incomplete.

## REFERENCES

- [1] Kotousov, A., Lazzarin, P., Berto, F., Harding, S., Effect of the thickness on elastic deformation and quasi-brittle fracture of plate components, *Eng. Fract. Mech.*, 77 (2010) 1665-1681.
- [2] Kotousov, A., Lazzarin, P., Berto, F., Pook, L. P., Three-dimensional stress states at crack tip induced by shear and anti-plane loading, *Eng. Fract. Mech.*, 108 (2013) 65-74.
- [3] Pook, L. P., Campagnolo, A., Berto, F., Lazzarin, P., Coupled fracture mode of a cracked plate under anti-plane loading, *Eng. Fract. Mech.*, (2015) doi:10.1016/j.engfracmech.2014.12.021.
- [4] Pook, L. P., A 50-year retrospective review of three-dimensional effects at cracks and sharp notches, *Fatigue Fract. Engng. Mater. Struct.*, 36 (2013) 699-723.
- [5] Bažant, Z. P., Estenssoro, L. F., Surface singularity and crack propagation, *Int. J. Solids Struct.*, 15 (1979) 405-426.
- [6] Pook, L. P., Some implications of corner point singularities, *Eng. Fract. Mech.*, 48 (1994) 367-378.
- [7] Pook, L. P., *Linear elastic fracture mechanics for engineers. Theory and applications*, WIT Press, Southampton (UK), (2000).





- [8] Williams, M. L., On the stress distribution at the base of a stationary crack, *J. appl. Mech.*, 24 (1957) 109-114.
- [9] Benthem, J. P., The quarter-infinite crack in a half-space; alternative and additional solutions, *Int. J. Solids Struct.*, 16(2) (1980) 119-130.
- [10] Dhondt, G., On corner point singularities along a quarter circular crack subject to shear loading, *Int. J. Fract.*, 89 (1998) L13-L18.
- [11] Paris, P. C., Sih, G. C., Stress analysis of cracks, in: *Fracture toughness testing and its applications*, ASTM STP 381, American Society for Testing and Materials, Philadelphia (USA), (1965) 30-81.
- [12] Timoshenko, S. P., Goodier, J. N., *Theory of elasticity*, third ed., McGraw-Hill Book Company, New York (USA), (1970).
- [13] Berto, F., Lazzarin, P., Recent developments in brittle and quasi-brittle failure assessment of engineering materials by means of local approaches, *Mater. Sci. Eng. R*, 75 (2014) 1-48.
- [14] Lazzarin, P., Berto, F., Elices, M., Gómez, J., Brittle failures from U- and V-notches in mode I and mixed, I+II, mode. A synthesis based on the strain energy density averaged on finite size volumes, *Fatigue Fract. Engng Mater. Struct.*, 32 (2009) 671-684.
- [15] Torabi, A. R., Campagnolo, A., Berto, F., Mode II brittle fracture assessment of key-hole notches by means of the local energy, *J. Test. Eval.*, 44 (2016) doi: 10.1520/JTE20140295.
- [16] Torabi, A. R., Campagnolo, A., Berto, F., Local strain energy density to predict mode II brittle fracture in Brazilian disk specimens weakened by V-notches with end holes, *Mater. Design*, 69 (2015) 22-29.
- [17] Berto, F., Lazzarin, P., Yates, J. R., Multiaxial fatigue of V-notched steel specimens: A non-conventional application of the local energy method, *Fatigue Fract. Engng. Mater. Struct.*, 34 (2011) 921-943.
- [18] Berto, F., Campagnolo, A., Lazzarin, P., Fatigue strength of severely notched specimens made of Ti-6Al-4V under multiaxial loading, *Fatigue Fract. Engng. Mater. Struct.*, (2015) doi: 10.1111/ffe.12272.
- [19] Lazzarin, P., Berto, F., Zappalorto, M., Rapid calculations of notch stress intensity factors based on averaged strain energy density from coarse meshes: Theoretical bases and applications, *Int. J. Fatigue*, 32 (2010) 1559-1567.
- [20] Yosibash, Z., Shannon, S., Computing edge stress intensity functions (ESIFs) along circular 3-D edges, *Eng. Fract. Mech.*, 117 (2014) 127-151.
- [21] Omer, N., Yosibash, Z., On the path independency of the point-wise J integral in three dimensions, *Int. J. Fracture*, 136 (2005) 1-36.
- [22] Campagnolo, A., Berto, F., Lazzarin, P., The effects of different boundary conditions on three-dimensional cracked discs under anti-plane loading, *Eur. J. Mech. – A/Solids*, 50 (2015) 76-86.